A&A 581, A132 (2015)
DOI: 10.1051/0004-6361/201424165

Astronomy & Astrophysics

What powers Lyα blobs?★

Y. Ao[1,2], Y. Matsuda[1], A. Beelen[3], C. Henkel[4,5], R. Cen[6], C. De Breuck[7], P. J. Francis[8], A. Kovács[9], G. Lagache[10], M. Lehnert[11], M. Y. Mao[12,13,14], K. M. Menten[4], R. P. Norris[13], A. Omont[11], K. Tatemastu[1], A. Weiß[4], and Z. Zheng[15]

[1] National Astronomical Observatory of Japan, 2-21-1 Osawa, Mitaka, 181-8588 Tokyo, Japan
e-mail: yiping.ao@nao.ac.jp
[2] Purple Mountain Observatory, Chinese Academy of Sciences, 210008 Nanjing, PR China
[3] Institut d'Astrophysique Spatiale, Bât. 121, Université Paris-Sud, 91405 Orsay Cedex, France
[4] MPIfR, Auf dem Hügel 69, 53121 Bonn, Germany
[5] Astron. Dept., King Abdulaziz Univ., PO Box 80203, 21589 Jeddah, Saudi Arabia
[6] Princeton University Observatory, Princeton, NJ 08544, USA
[7] European Southern Observatory, Karl Schwarzschild Straße 2, 85748 Garching, Germany
[8] Research School of Astronomy and Astrophysics, The Australian National University, Canberra ACT 0200, Australia
[9] California Institute of Technology 301-17, 1200 E. California Blvd, Pasadena, CA 91125, USA
[10] Aix Marseille Université, CNRS, LAM (Laboratoire d'Astrophysique de Marseille) UMR 7326, 13388 Marseille, France
[11] Institut d'Astrophysique de Paris, CNRS and Université Pierre et Marie Curie, 98bis Bd Arago, 75014 Paris, France
[12] School of Mathematics and Physics, University of Tasmania, Private Bag 37 Hobart, 7001, Australia
[13] Joint Institute for VLBI, Postbus 2, 7990 AA Dwingeloo, The Netherlands
[14] Australia Telescope National Facility, CSIRO Astronomy and Space Science, PO Box 76, Epping, NSW 1710, Australia
[15] Department of Physics and Astronomy, University of Utah, Salt Lake City, UT 84112, USA

Received 9 May 2014 / Accepted 20 July 2015

ABSTRACT

Lyα blobs (LABs) are spatially extended Lyα nebulae seen at high redshift. The origin of Lyα emission in the LABs is still unclear and under debate. To study their heating mechanism(s), we present Australia Telescope Compact Array (ATCA) observations of the 20 cm radio emission and *Herschel* PACS and SPIRE measurements of the far-infrared (FIR) emission toward the four LABs in the protocluster J2143-4423 at $z = 2.38$. Among the four LABs, B6 and B7 are detected in the radio with fluxes of 67 ± 17 μJy and 77 ± 16 μJy, respectively, and B5 is marginally detected at 3σ (51 ± 16 μJy). For all detected sources, their radio positions are consistent with the central positions of the LABs. Among them, B6 and B7 are obviously also detected in the FIR. By fitting the data with different templates, we obtained redshifts of $2.20^{+0.30}_{-0.35}$ for B6 and $2.20^{+0.45}_{-0.30}$ for B7, which are consistent with the redshift of the Lyα emission within uncertainties, indicating that both FIR sources are likely associated with the LABs. The associated FIR emission in B6 and B7 and high star formation rates strongly favor star formation in galaxies as an important powering source for the Lyα emission in both LABs. However, the other two, B1 and B5, are predominantly driven by the active galactic nuclei or other sources of energy still to be specified, but not mainly by star formation. In general, the LABs are powered by quite diverse sources of energy.

Key words. galaxies: formation – galaxies: high-redshift – galaxies: ISM – galaxies: active – infrared: galaxies

1. Introduction

High-redshift, star-forming galaxies are becoming an important probe of galaxy formation, reionization, and cosmology (Robertson et al. 2010; Shapley 2011). A popular method for finding high-redshift, star-forming galaxies is to target their often bright Lyα emission (Partridge & Peebles 1967). This emission can be easily detected in narrowband imaging surveys, and can be further confirmed by spectroscopic observations (Hu et al. 1998; Ouchi et al. 2008; Yamada et al. 2012a,b). In addition to discovering numerous Lyα emitters (LAEs), a particular class of objects, also known as "Lyα blobs" (LABs), has been most commonly found in the dense environment of star-forming galaxies at high redshift, and these are very extended (30 to 200 kpc) and Lyα-luminous (10^{43} to 10^{44} erg s^{-1}; see, e.g., Francis et al. 1996; Steidel et al. 2000; Palunas et al. 2004; Matsuda et al. 2004, 2009, 2011; Dey et al. 2005; Saito et al. 2006; Yang et al. 2009, 2010; Erb et al. 2011; Prescott et al. 2012a, 2013; Bridge et al. 2013). In contrast to the large Lyα nebulae surrounding some high-redshift radio galaxies (e.g., Reuland et al. 2003; Venemans et al. 2007), these objects do not always have obvious sources for energy responsible for their strong emission.

While the LABs' preferential location in overdense environments indicates an association with massive galaxy formation, the origin of Lyα emission in the LABs is still unclear and under debate (Faucher-Giguere et al. 2010; Cen & Zheng 2013; Yajima et al. 2013). Proposed sources have generally fallen into two categories: cooling radiation from cold streams of gas accreting onto galaxies (e.g., Haiman et al. 2000; Dijkstra & Loeb 2009; Goerdt et al. 2010), as well as photoionization and recombination from starbursts or active galactic nuclei (AGNs; e.g., Taniguchi & Shioya 2000; Furlanetto et al. 2005; Mori & Umemura 2006; Zheng et al. 2011). Supporting evidence for the cooling flow scenario comes from those LABs lacking any visible power source (e.g., Nilsson et al. 2006; Smith & Jarvis 2007). Ionizing photons from young stars in star-forming galaxies or AGNs can ionize neutral hydrogen atoms and the subsequent recombination gives off Lyα emission. The resonant scattering of Lyα photons in the circumgalactic medium makes the emission extended (Geach et al. 2005, 2009; Colbert et al. 2006, 2011; Beelen et al. 2008; Webb et al. 2009; Zheng et al. 2011; Cen & Zheng 2013; Overzier et al. 2013).

★ *Herschel* (Pilbratt et al. 2010) is an ESA space observatory with science instruments provided by European-led Principal Investigator consortia and with important participation from NASA.

Except for cooling flows and photoionization from star-forming galaxies or AGNs, other possible mechanisms, such as galactic super-winds and obscured AGNs, are also proposed to explain the nature of LABs (e.g., Ohyama et al. 2003; Wilman et al. 2005; Colbert et al. 2006; Matsuda et al. 2007). All these sources of energy may be activated in an environment in which violent interactions are frequent between gas-rich galaxies as expected in overdense regions at high redshift (Matsuda et al. 2009, 2011; Prescott et al. 2012b; Kubo et al. 2013).

The 110 Mpc filament with 37 LAEs related to the protocluster J2143-4423 at $z = 2.38$ (Francis et al. 1996, 2004; Palunas et al. 2004) is one of the largest known structures at high redshift, and this field also includes four large extended LABs with extensions of ~50 kpc and above, named B1, B5, B6, and B7. In this paper, we present our deep radio observations and *Herschel* released far-infrared (FIR) data in J2143-4423 to study the powering source of these LABs. Throughout this paper, we use a Λ cosmology with $H_0 = 67.3$ km s^{-1} Mpc^{-1}, $\Omega_\Lambda = 0.685$, and $\Omega_\mathrm{m} = 0.315$ (Planck Collaboration XVI 2014), and 1″ corresponds to 8.37 kpc at $z = 2.38$.

2. Observations

2.1. ATCA observations

We observed J2143-4423 with the Australia Telescope Compact Array (ATCA)[1] in its extended configuration 6A. During the observations from 2009 June 14 to 17, only five out of six antennas were available. The observations were performed at a central frequency of 1.75 GHz. We used the Compact Array Broadband Backend (Wilson et al. 2011) in a wideband mode, with a total bandwidth of 2 GHz and a channel width of 1 MHz. The nearby source PKS 2134-470 served as a gain calibrator. Absolute fluxes were calibrated with the ATCA standard PKS 1934-638. The total observing time was about 70 h.

The data were reduced with the MIRIAD software package. Although the observations were carried out with a total bandwidth of 2 GHz, the effective bandwidth was about 489 MHz with a central frequency of 1.51 GHz. We carefully flagged the channels affected by radio frequency interference (RFI) by checking the visibility data sorted by time, channels, and baselines. The image was deconvolved with MIRIAD task MFCLEAN, and task SELFCAL was used to reduce the noise from strong radio continuum sources. We first created cleaned images in a normal procedure and made model images for the strong sources. The models were used as inputs for task SELFCAL to perform self-calibration of visibility data. We ran this cycle three times, and then obtained the model images to create the visibility data with self-calibration, which were used to make the final images. The noise of the images after applying self-calibration was about one order of magnitude lower than that without self-calibration. The field of view was about 31 arcmins and the synthesized beam size was 7.8″ × 4.8″. The noise was about 15 μJy/beam before applying primary beam correction.

2.2. Archival Herschel observations

Herschel observations toward J2143-4423 were carried out with PACS (Poglitsch et al. 2010) at 100 and 160 μm and SPIRE (Griffin et al. 2010) at 250, 350, and 500 μm in 2010 to 2011. J2143-4423 was imaged in a field size of 15′ × 15′ for each band, and the observing time was ~2.9 h for PACS (*Herschel* OD: 686) and ~0.6 h for SPIRE (*Herschel* OD: 558). The level 2.5 product for PACS and the level 2 product for SPIRE from the pipeline procedures are used for our data analysis. Source photometry is carried out using DAOphot algorithm in the *Herschel* interactive processing environment (HIPE). We apply beam correction, colour correction, and aperture correction for a spectral index of −2 and adopt a flux calibration error of 5% at PACS bands and 7% at SPIRE bands, as recommended in the PACS and SPIRE Observers Manual. The full width at half power (FWHP) beam sizes are 6.8″ at 100 μm, 11.4″ at 160 μm, 17.6″ at 250 μm, 23.9″ at 350 μm, and 35.2″ at 500 μm, respectively.

3. Results

3.1. Radio emission from ATCA observations

In Fig. 1a we present the radio continuum emission images at 20 cm from the ATCA. Among the four LABs, B6 and B7 are detected with fluxes of 67 ± 17 μJy and 77 ± 16 μJy, respectively, and B5 is marginally detected at 3σ (51 ± 16 μJy). For all detected sources, their positions are consistent with the central positions of the LABs. The only undetected source is B1.

3.2. FIR emission from Herschel observations

All four LABs are observed with *Herschel* PACS at 100 and 160 μm and SPIRE at 250, 350, and 500 μm, and the images are shown in Figs. 1c−g. The observed flux densities are calculated for the areas within the blue circles, as shown in Fig. 1, and are listed in Table 1. B1 is not detected but contaminated by a nearby strong source about 20″ in the northwest, which is the background QSO LBQS2138-4427 at $z = 3.2$ (Francis & Hewett 1993), and its emission features at different FIR bands appear to reach out to B1 from this location. There is no FIR counterpart for B5 in any *Herschel* band.

3.3. Redshifts of the FIR sources

To estimate the redshift of the FIR sources associated with B6 and B7, we try to fit the data with the SEDs of different templates (Polletta et al. 2007) at different redshifts and find that the starburst templates can well reproduce the data. With the observational data and the SEDs of the templates, the minimum reduced χ^2 value for each redshift can be calculated and the corresponding probability can be estimated. In this analysis, we include five *Herschel* band, APEX 870 μm data (Beelen et al. 2008), and *Spitzer* MIPS 24 μm data (Colbert et al. 2006).

Among four typical templates, Arp 220, M 82, Mrk 231, and NGC 6240, we find that the spectral energy distribution of starburst galaxies NGC 6240 and Arp 220 fit the data best, and Mrk 231 does not fit well because it has warm IR emission from its AGN, which is not really consistent with the data. Figure 2 shows the probability distribution against redshift for both LABs. The estimated redshifts are $2.20^{+0.30}_{-0.35}$ for B6 and $2.20^{+0.45}_{-0.30}$ for B7, respectively. Considering the uncertainty of this method to determine the redshifts, both values are consistent with the Lyα redshift of 2.38 of the LABs. Adopting the number count study of *Herschel* sources in Clements et al. (2010), the probability of finding a 350 μm source with a flux greater than 40 mJy within 20 arcsec is 2%. With this low number density of strong FIR sources and the positional coincidence of the LABs

[1] The Australia Telescope Compact Array is part of the Australia Telescope, which is funded by the Commonwealth of Australia for operation as a national facility managed by CSIRO.

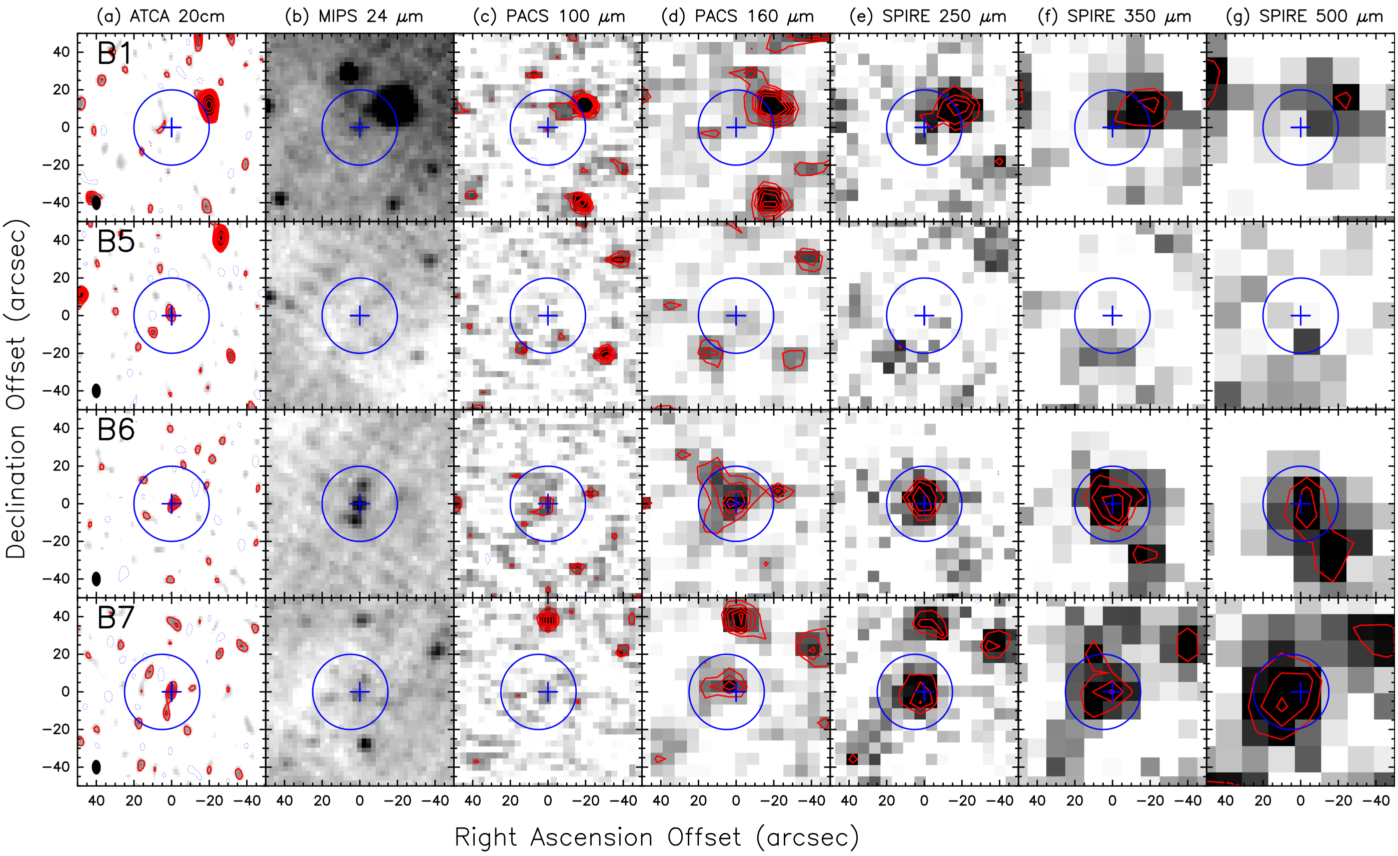

Fig. 1. ATCA 20 cm, *Spitzer* MIPS 24 μm, and *Herschel* PACS and SPIRE data for the four Lyα blobs (LABs) in J2143-4423. **a)** Contours and gray scale maps of ATCA radio emission. The contours are −2, 2, 3, 4, 5, and 6 × 15 μJy (1σ), with a synthesized beam of 7.8″ × 4.8″, which is shown in the lower left corner of each panel. **b)** Gray maps of *Spitzer* MIPS 24 μm emission (Colbert et al. 2006). **c)–g)** Contours and gray scale maps of *Herschel* FIR emission. The contours are -2σ, 2σ, 3σ, 4σ, 5σ, and 6σ (see Sect. 2.2 for the noise level of each band). A circle with a diameter of 40″ is shown in each panel. The circles in B7 are in an off-center position (5″, 0″) to cover the most FIR emission. All sources are centered on the positions of the four LABs (see Colbert et al. 2006) as shown with plus signs in each panel. All offsets are relative to the positions of the LABs.

Table 1. Observational and derived parameters toward the four LABs.

Source	20 cm[a] [μJy]	100 μm [mJy]	160 μm [mJy]	250 μm [mJy]	350 μm [mJy]	500 μm [mJy]	$L_{\rm FIR}$[b] [10^{12} $L_\odot$]	$M_{\rm dust}$ [10^8 $M_\odot$]
B1	<51	<4.2	<9.0	<17.9	<19.6	<22.5	<2.8	
B5	51 ± 16	<2.1	<11.1	<17.5	<18.7	<19.8	<2.5	
B6	67 ± 17	13.2 ± 3.2	53.9 ± 8.0	49.7 ± 9.0	53.7 ± 10.7	36.7 ± 10.3	10.0 ± 1.9	3.2 ± 0.6
B7	77 ± 16	12.9 ± 4.0	33.5 ± 10.0	41.6 ± 7.8	48.0 ± 10.6	39.2 ± 8.6	8.6 ± 2.3	5.0 ± 1.0

Notes. The wavelengths shown in this table are the redshifted values. [(a)] Measured fluxes have been modified by a primary beam correction (less than 15%). [(b)] The total luminosities are calculated between rest-frame wavelengths of 40 μm to 200 μm from the dust models (see Sect. 3.4 for details). The 3σ upper limits are given for undetected sources.

with strong FIR sources, the FIR sources are very likely associated with the LABs. Nevertheless, future spectroscopic observations from molecular lines at millimeter or from forbidden lines at near-infrared will be quite important to confirm this finding. In the following sections, we adopt the Lyα redshift of 2.38 for the LABs.

3.4. Dust properties

For B6 and B7, we have included the measurements from the five *Herschel* bands, as well as the 870 μm data taken from Beelen et al. (2008) in the dust continuum analysis, using a single-component dust model as described in Weiß et al. (2007). *Spitzer* MIPS 24 μm data (Colbert et al. 2006) are not used in the model fitting because they are strongly affected by PAH features, but are shown in Fig. 3 to allow for a better comparison with overlaid templates. We find a dust temperature, $T_{\rm dust}$, of 70 ± 5 K and a dust mass, $M_{\rm dust}$, of $(3.2 \pm 0.8) \times 10^8$ $M_\odot$ for B6, and $T_{\rm dust}$ = 70 ± 5 K and $M_{\rm dust} = (5.0 \pm 1.0) \times 10^8$ $M_\odot$ for B7, respectively. The implied FIR luminosities are $L_{\rm FIR} = (10.0 \pm 1.9) \times 10^{12}$ $L_\odot$ for B6, and $L_{\rm FIR} = (8.6 \pm 2.3) \times 10^{12}$ $L_\odot$ for B7, respectively, where $L_{\rm FIR}$ is integrated from 40 μm to 200 μm in the rest frame. The upper $L_{\rm FIR}$ limits for both B1 and B5 are ∼2.5–2.8 × 10^{12} $L_\odot$.

3.5. Star formation rates

Here we derive the star formation rates from the Lyα, far-infrared, and radio luminosities. To estimate the star formation rate (SFR) from the Lyα luminosity, we first assume that

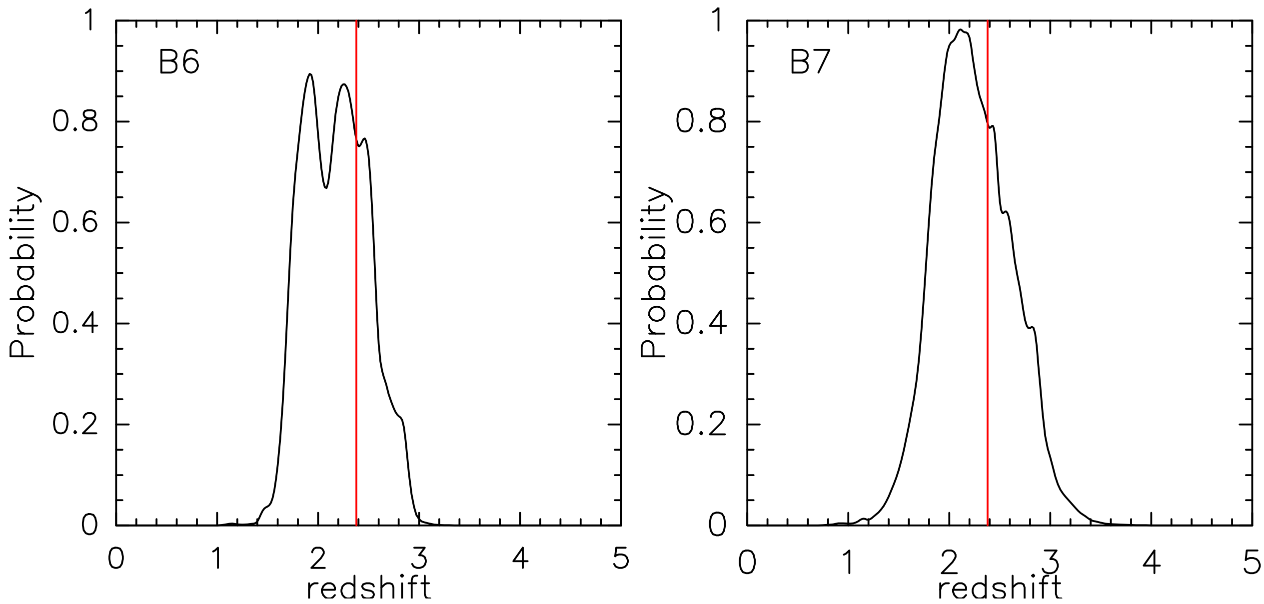

Fig. 2. Probability as a function of redshift for B6 and B7. NGC 6240 and Arp 220 are adopted as the most appropriate starburst templates for B6 and B7, respectively. A red vertical line denotes a redshift of 2.38 for Lyα emission.

Table 2. Derived star formation rates toward the four LABs.

Source	$SFR(L_{\rm FIR})$ [$M_\odot$/yr]	$SFR(L_{1.4\ \rm GHz})$ [$M_\odot$/yr]	log $L_{\rm Ly\alpha}$ [a] [erg s^{-1}]	SFR(Lyα) [$M_\odot$/yr]
B1	<480	<1090	43.9	79
B5	<430	1090 ± 340	43.8	63
B6	1700 ± 320	1430 ± 360	43.8	63
B7	1460 ± 390	1650 ± 340	43.5	32

Notes. [(a)] The Lyα luminosities are adopted from Colbert et al. (2006).

star formation (SF) powers the observed Lyα flux. We use an unreddened Lyα/Hα ratio of 8:1 and the conversion factor between Hα luminosity and SFR (Kennicutt 1998), yielding $SFR({\rm Ly}\alpha)/(M_\odot/{\rm yr}) = L_{\rm Ly\alpha}/(10^{42}\ {\rm erg\,s^{-1}})$. This provides a lower limit because the extinction of Lyα emission caused by dust largely reduces the observed Lyα luminosity. With the FIR luminosity derived from *Herschel* data, we can estimate the SFR using the relation $SFR(L_{\rm FIR})/(M_\odot/{\rm yr}) = 1.7 \times L_{\rm FIR}/(10^{10}\ L_\odot$; Kennicutt 1998). If the observed radio emission, with a rest wavelength of 6 cm, is dominated by free-free emission in HII regions, one can also relate the SFR with the relation $SFR(L_{1.4\ \rm GHz})/(M_\odot/{\rm yr}) = 5.52 \times 10^{-22}\ L_{1.4\ \rm GHz}/({\rm W\,Hz^{-1}})$ (Bell 2003). The radio luminosity at 1.4 GHz at the rest frame can be estimated from the observed flux at 1.51 GHz by assuming a relation $S \propto \nu^\alpha$, where S is the flux density and the typical spectral index α of -0.8 is commonly adopted for the SMGs (e.g., Ivison et al. 2010). These values are listed in Table 2.

4. Discussion and conclusions

A high detection rate of radio emission (three out of four) around LABs suggests that most LABs do not originate from cooling radiation. Instead, photoionization from starbursts or AGNs may power the LABs in most cases. The high rate of FIR detections (two out of four) points to a star-formation origin of the LABs. The SEDs of B6 and B7 can be well described by starburst dominated templates, as shown in Fig. 3, further supporting Lyα emission related to the SF in the LABs. In B6 and B7, the SFRs derived from Lyα fluxes are far below those estimated from FIR luminosities (Table 2). This suggests that the dust greatly reduces the measured Lyα flux. Comparing the different SFRs, the dust absorption optical depth of the Lyα emission becomes ~3.1−3.6. The SFRs estimated from the FIR and radio luminosities are comparable, indicating that the radio emission is dominated by SF, not by AGNs. The energetic starbursts can provide enough ionizing photons to ionize neutral hydrogen atoms in the interstellar medium (ISM), and each subsequent recombination has a probability of ~2/3 of ending up a Lyα photon (Partridge & Peebles 1967). After escaping the galaxy's ISM, these Lyα photons can be resonantly scattered by neutral hydrogen atoms in the intergalactic medium (IGM), which tends to make the Lyα emission extended (Zheng et al. 2011).

Cen & Zheng (2013) propose an SF-based model and predict that LABs at high redshift correspond to protoclusters containing the most massive galaxies and cluster halos in the early Universe as well as ubiquitous strong infrared sources undergoing extreme starbursts. This may be supported by the multiple Spitzer/MIPS sources detected in both LABs (see Fig. 1b, Colbert et al. 2006, 2011). Indeed, Prescott et al. (2012b) suggest that LABs may be the seeds of galaxy clusters by resolving the galaxies within a LAB at z = 2.7. The strong FIR emission and the inferred high SFRs support the presence of a strong starburst in both B6 and B7. However, AGN-dominated templates like Mrk 231 cannot reproduce the data well (see Sect. 3.3), suggesting that the SF instead of AGN may power the Lyα emission in both LABs. The model also predicts that the most luminous FIR source in each LAB likely represents the gravitational center of the protocluster. Figures 1c−g shows that the FIR emission indeed peaks in the centers of B6 and B7. The radio continuum emission is detected exclusively in the centers, which suggests that the source with most luminous FIR emission (therefore highest SFR) is in the gravitational center of each LAB. Another very important prediction of this model is that the Lyα emission from photons that escape the galaxy are expected to be significantly polarized, which has been confirmed by Hayes et al. (2011) for the first time toward LAB1 in the SSA22 field, supporting models with central power sources. Adopting a gas-to-dust mass ratio

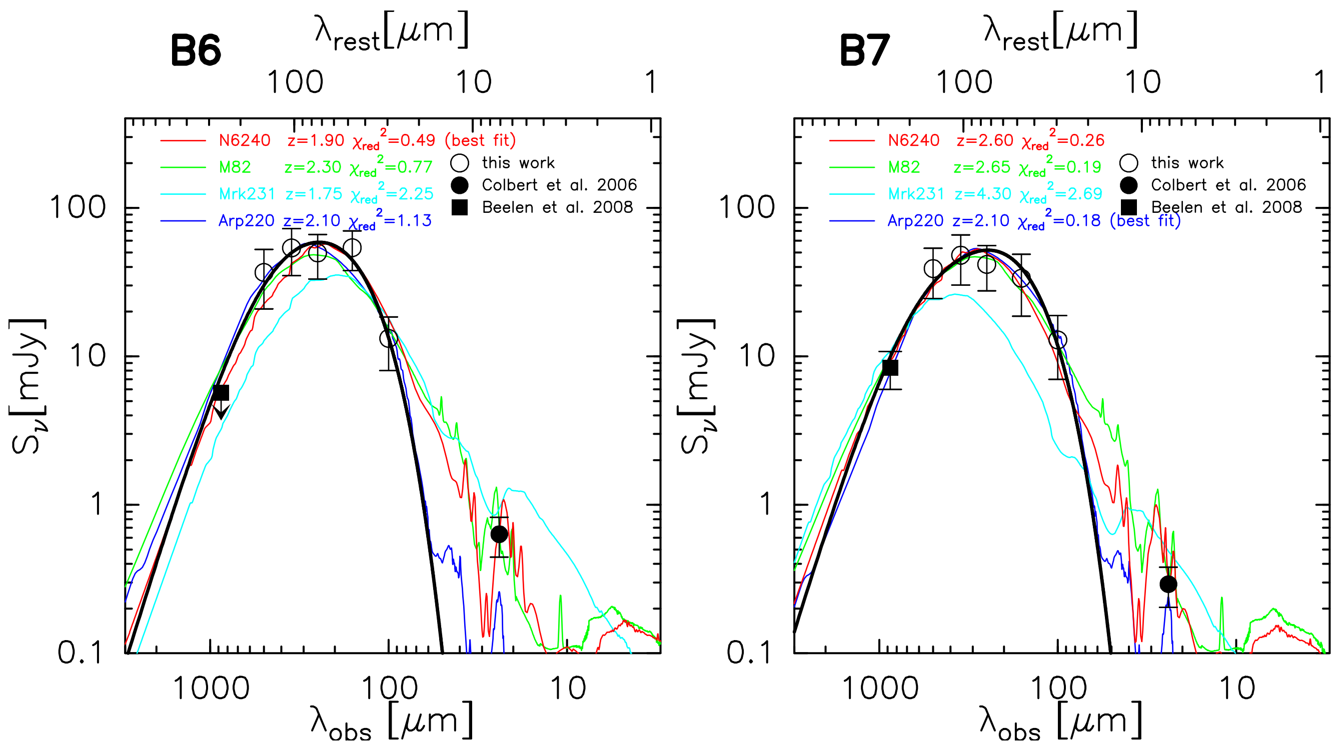

Fig. 3. Single-component dust models for B6 and B7 (a redshift of 2.38 is adopted). The black solid lines show the thermal dust continuum emission of the 70 K dust components for both B6 and B7. The open circles represent the measurements at our five *Herschel* bands and the filled circles indicate the flux densities at 24 μm (Colbert et al. 2006). The filled square denotes the flux density (or its upper limit) at 870 μm, taken from Beelen et al. (2008). The wavelengths at the rest frame are labeled on the top. For the single-component dust models adopted in the figure (see Sect. 3.4 for details of the dust models.), the χ^2 values are 1.1 for B6 and 1.0 for B7, respectively. In Sect. 3.3, four typical starburst templates, NGC 6240, M 82, Mrk 231, and Arp 220 (Polletta et al. 2007), are adopted to estimate the redshifts for B6 and B7, and their best fits are overlaid in colored lines.

of 150 and the SFRs estimated above, the timescales of B6 and B7 are relatively short (~100 Myr), which is much shorter than the galaxy building timescale. Note that this timescale is a lower limit because (1) the LABs may have been alive for a while now; and (2) additional gas may be continuously accreted. In any case, the LABs are visible only for a short time interval during the lifetime of their parent clusters.

Note that the so-called "SF-based model" proposed by Cen & Zheng (2013) also includes AGN powering or any central powering. The morphologies of the Lyα emission of the four LABs are quite different (Palunas et al. 2004): B1 and B5 have core-like structures, while B6 and B7 are characterized by diffuse and extended emission with physical sizes of ~60−70 kpc. The latter may be driven by multiple sources, as suggested by the MIPS data, and are consistent with the SF-based model. There is no clear FIR emission detected around B1 and B5. Therefore, the Lyα emission in both LABs is unlikely predominantly triggered by SF. Overzier et al. (2013) conclude that in B1 the photoionization from an AGN is the main driver of Lyα emission. However, Francis et al. (2013) shows that the observed Lyα emission in B1 is of complex origin, dominated by the sum of the emission from the sub-haloes where the cold gas is most likely being lit up by a combination of tidally triggered star formation, bow shocks, resonant scattering of Lyα from the filament collisions, and tidal stripping of the gas. Radio emission is tentatively detected in B5 and, therefore, the AGN may also power the Lyα emission. Among the four LABs in J2143-4423, two of them, B6 and B7, are mainly driven by SF. However, the other two LABs, B1 and B5, without clear FIR detection, are predominantly driven by the AGNs or other sources of energy still to be specified, but not mainly by star formation. We thus conclude that LABs must be powered by quite diverse sources of energy.

With its high angular resolution and superb sensitivity, future observations with the Large Atacama Millimeter Array (ALMA) will reveal more details about the nature of LABs, such as testing the predictions of models where the ionization is provided by intense star formation and confirming the significantly polarized dust emission at mm/submm wavelength.

Acknowledgements. We thank the anonymous referee for valuable comments that improved this manuscript. Y.A. acknowledges partial support by NSFC grant 11373007 and Youth Innovation Promotion Association CAS. R.C. is supported in part by NASA grant NNX11AI23G. Y.M. acknowledges support from JSPS KAKENHI Grant Number 20647268. Z.Z. was partially supported by NSF grant AST-1208891 and NASA grant NNX14AC89G. This research has made use of NASA's Astrophysical Data System (ADS). PACS has been developed by a consortium of institutes led by MPE (Germany) and including UVIE (Austria); KU Leuven, CSL, IMEC (Belgium); CEA, LAM (France); MPIA (Germany); INAF-IFSI/OAA/OAP/OAT, LENS, SISSA (Italy); IAC (Spain). This development has been supported by the funding agencies BMVIT (Austria), ESA-PRODEX (Belgium), CEA/CNES (France), DLR (Germany), ASI/INAF (Italy), and CICYT/MCYT (Spain). SPIRE has been developed by a consortium of institutes led by Cardiff University (UK) and including Univ. Lethbridge (Canada); NAOC (China); CEA, LAM (France); IFSI, Univ. Padua (Italy); IAC (Spain); Stockholm Observatory (Sweden); Imperial College London, RAL, UCL-MSSL, UKATC, Univ. Sussex (UK); and Caltech, JPL, NHSC, Univ. Colorado (USA). This development has been supported by national funding agencies: CSA (Canada); NAOC (China); CEA, CNES, CNRS (France); ASI (Italy); MCINN (Spain); SNSB (Sweden); STFC, UKSA (UK); and NASA (USA).

References

Beelen, A., Omont, A., Bavouzet, N., et al. 2008, A&A, 485, 645
Bell, E. F. 2003, ApJ, 586, 794
Bridge, C. R., Blain, A., Borys, C. J. K., et al. 2013, ApJ, 769, 91
Cen, R., & Zheng, Z. 2013, ApJ, 775, 112
Clements, D. L., Rigby, E., Maddox, S., et al. 2010, A&A, 518, L8
Colbert, J. W., Teplitz, H., Francis, P., et al. 2006, ApJ, 637, L89
Dey, A., Bian, C., Soifer, B. T., et al. 2005, ApJ, 629, 654
Dijkstra, M., & Loeb, A. 2009, MNRAS, 400, 1109
Erb, D. K., Bogosavljević, M., & Steidel, C. C. 2011, ApJ, 740, L31
Faucher-Giguère, C.-A., Kereš, D., Dijkstra, M., Hernquist, L., & Zaldarriaga, M. 2010, ApJ, 725, 633
Francis, P. J., & Hewett, P. C. 1993, AJ, 105, 1633
Francis, P. J., Woodgate, B. E., Warren, S. J., et al. 1996, ApJ, 457, 490
Francis, P. J., Palunas, P., Teplitz, H. I., Williger, G. M., & Woodgate, B. E. 2004, ApJ, 614, 75
Francis, P. J., Dopita, M. A., Colbert, J. W., et al. 2013, MNRAS, 428, 28
Furlanetto, S. R., Schaye, J., Springel, V., & Hernquist, L. 2005, ApJ, 622, 7
Geach, J. E., Matsuda, Y., Smail, I., et al. 2005, MNRAS, 363, 1398
Geach, J. E., Alexander, D. M., Lehmer, B. D., et al. 2009, ApJ, 700, 1
Goerdt, T., Dekel, A., Sternberg, A., et al. 2010, MNRAS, 407, 613
Griffin, M. J., Abergel, A., Abreu, A., et al. 2010, A&A, 518, L3
Haiman, Z., Spaans, M., & Quataert, E. 2000, ApJ, 537, L5
Hayes, M., Scarlata, C., & Siana, B. 2011, Nature, 476, 304
Hu, E. M., Cowie, L. L., & McMahon, R. G. 1998, ApJ, 502, L99
Ivison, R. J., Magnelli, B., Ibar, E., et al. 2010, A&A, 518, L31
Kennicutt, R. C., Jr. 1998, ARA&A, 36, 189
Kubo, M., Uchimoto, Y. K., Yamada, T., et al. 2013, ApJ, 778, 170
Matsuda, Y., Yamada, T., Hayashino, T., et al. 2004, AJ, 128, 569
Matsuda, Y., Iono, D., Ohta, K., et al. 2007, ApJ, 667, 667
Matsuda, Y., Nakamura, Y., Morimoto, N., et al. 2009, MNRAS, 400, L66
Matsuda, Y., Yamada, T., Hayashino, T., et al. 2011, MNRAS, 410, L13
Mori, M., & Umemura, M. 2006, Nature, 440, 644
Nilsson, K. K., Fynbo, J. P. U., Møller, P., Sommer-Larsen, J., & Ledoux, C. 2006, A&A, 452, L23
Ohyama, Y., Taniguchi, Y., Kawabata, K. S., et al. 2003, ApJ, 591, L9
Ouchi, M., Shimasaku, K., Akiyama, M., et al. 2008, ApJS, 176, 301
Overzier, R. A., Nesvadba, N. P. H., Dijkstra, M., et al. 2013, ApJ, 771, 89
Palunas, P., Teplitz, H. I., Francis, P. J., Williger, G. M., & Woodgate, B. E. 2004, ApJ, 602, 545
Partridge, R. B., & Peebles, P. J. E. 1967, ApJ, 147, 868
Planck Collaboration XVI. 2014, A&A, 571, A16
Poglitsch, A., Waelkens, C., Geis, N., et al. 2010, A&A, 518, L2
Polletta, M., Tajer, M., Maraschi, L., et al. 2007, ApJ, 663, 81
Prescott, M. K. M., Dey, A., & Jannuzi, B. T. 2012a, ApJ, 748, 125
Prescott, M. K. M., Dey, A., Brodwin, M., et al. 2012b, ApJ, 752, 86
Prescott, M. K. M., Dey, A., & Jannuzi, B. T. 2013, ApJ, 762, 38
Reuland, M., van Breugel, W., Röttgering, H., et al. 2003, ApJ, 592, 755
Riechers, D. A., Bradford, C. M., Clements, D. L., et al. 2013, Nature, 496, 329
Robertson, B. E., Ellis, R. S., Dunlop, J. S., McLure, R. J., & Stark, D. P. 2010, Nature, 468, 49
Saito, T., Shimasaku, K., Okamura, S., et al. 2006, ApJ, 648, 54
Shapley, A. E. 2011, ARA&A, 49, 525
Smith, D. J. B., & Jarvis, M. J. 2007, MNRAS, 378, L49
Spergel, D. N., Bean, R., Doré, O., et al. 2007, ApJS, 170, 377
Steidel, C. C., Adelberger, K. L., Shapley, A. E., et al. 2000, ApJ, 532, 170
Taniguchi, Y., & Shioya, Y. 2000, ApJ, 532, L13
Tielens, A. G. G. M. 2005, The Physics and Chemistry of the Interstellar Medium (Cambridge, UK: Cambridge University Press)
Venemans, B. P., Röttgering, H. J. A., Miley, G. K., et al. 2007, A&A, 461, 823
Webb, T. M. A., Yamada, T., Huang, J.-S., et al. 2009, ApJ, 692, 1561
Weiß, A., Downes, D., Neri, R., et al. 2007, A&A, 467, 955
Wilman, R. J., Gerssen, J., Bower, R. G., et al. 2005, Nature, 436, 227
Wilson, W. E., Ferris, R. H., Axtens, P., et al. 2011, MNRAS, 416, 832
Yajima, H., Li, Y., & Zhu, Q. 2013, ApJ, 773, 151
Yamada, T., Matsuda, Y., Kousai, K., et al. 2012a, ApJ, 751, 29
Yamada, T., Nakamura, Y., Matsuda, Y., et al. 2012b, AJ, 143, 79
Yang, Y., Zabludoff, A., Tremonti, C., Eisenstein, D., & Davé, R. 2009, ApJ, 693, 1579
Yang, Y., Zabludoff, A., Eisenstein, D., & Davé, R. 2010, ApJ, 719, 1654
Zheng, Z., Cen, R., Weinberg, D., Trac, H., & Miralda-Escudé, J. 2011, ApJ, 739, 62